Volume 23
Number 1
January 2021
Pages 1–190

Environmental Science
Processes & Impacts

rsc.li/espi

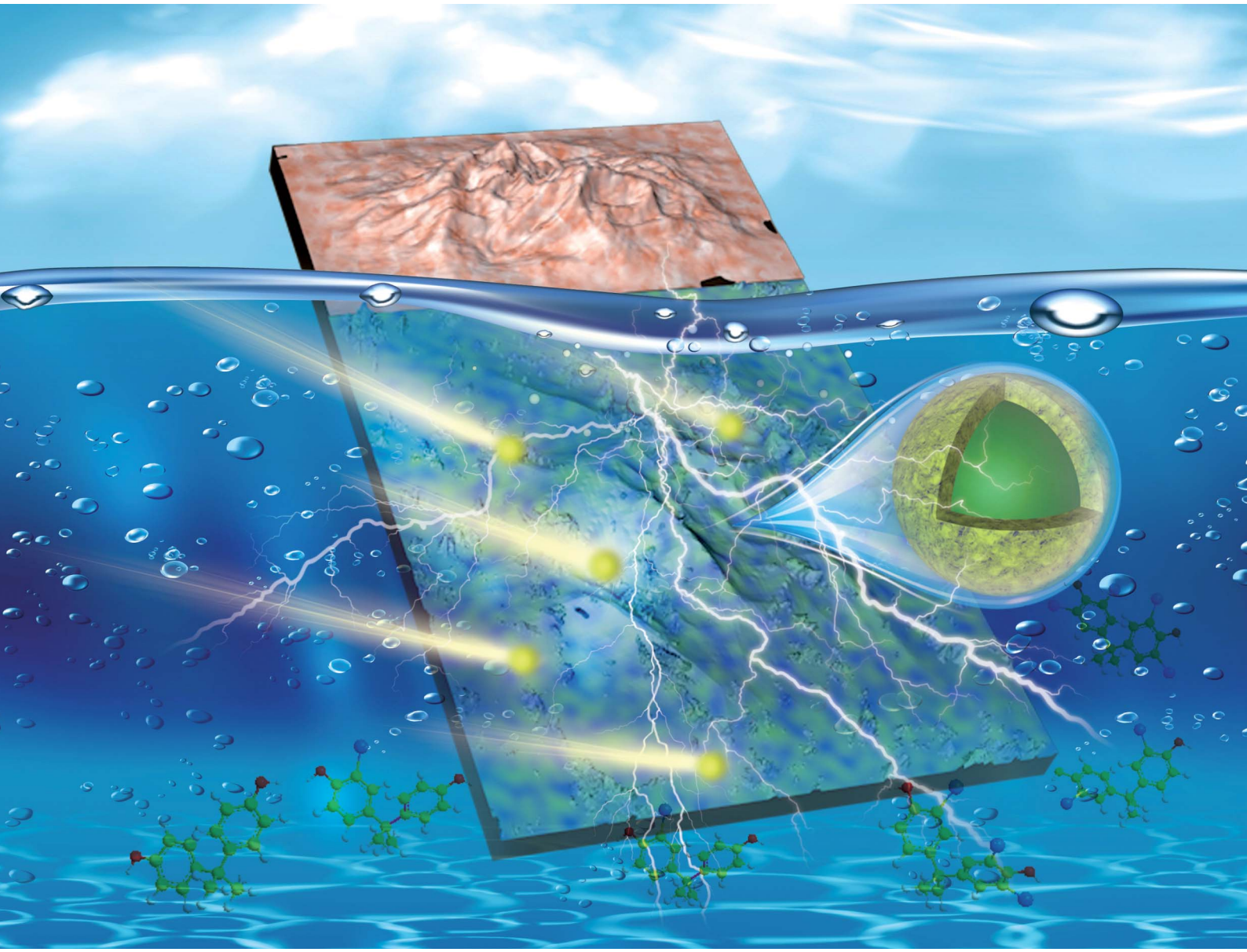

ISSN 2050-7887

ROYAL SOCIETY OF CHEMISTRY

PAPER

Yin Zhong *et al.*

Enhanced tetrabromobisphenol A debromination by nanoscale zero valent iron particles sulfidated with S^0 dissolved in ethanol

Environmental Science Processes & Impacts

PAPER

View Article Online
View Journal | View Issue

Cite this: *Environ. Sci.: Processes Impacts*, 2021, **23**, 86

Enhanced tetrabromobisphenol A debromination by nanoscale zero valent iron particles sulfidated with S^0 dissolved in ethanol†

Heli Wang,[ab] Yin Zhong, *[a] Xifen Zhu,[ab] Dan Li,[abd] Yirong Deng,[abe] Weilin Huang[c] and Ping'an Peng[a]

Modification of nanoscale zero-valent iron (nZVI) with reducing sulfur compounds has proven to improve the reactivity of nZVI towards recalcitrant halogenated organic contaminants. In this study, we develop a novel method for the preparation of sulfidated nZVI (S-nZVI) with S^0 (a low cost and available reducing sulfur agent) dissolved in ethanol under mild conditions and apply it for the transformation of tetrabromobisphenol A (TBBPA), a potential persistent organic pollutant. Surface analysis shows that S^0 dissolved in ethanol has been successfully doped into nZVI *via* a reaction with Fe^0 to form a relatively homogeneous layer of FeS/FeS_2 on the nZVI surface. The H_2 production test and the electrochemical analysis show that the FeS/FeS_2 layer not only slows the H_2 evolution reaction but also enhances the electron transfer. Debromination kinetics indicate that the resulting S-nZVI with a S/Fe ratio of 0.015–0.05 possesses higher debromination activity for TBBPA and its debromination products (*i.e.*, tri-BBPA, di-BBPA, mono-BBPA and BPA) in comparison with nZVI. Among them, S-nZVI at a S/Fe of 0.025 ($S\text{-nZVI}^{S\text{-}0.025}$) has the greatest debromination rate constant (k_{obs}) of $1.19 \pm 0.071\ h^{-1}$ for TBBPA. It debrominates TBBPA at a faster rate than other conventional S-nZVI made from Na_2S and $Na_2S_2O_4$ and has been successfully applied in the treatment of TBBPA-spiked environmental water samples (including river water, groundwater, and tap water). The results suggest that the modification of nZVI with S^0 dissolved in ethanol is a simple, safe, inexpensive, and effective sulfidation technique, which can be applied for the large-scale production of S-nZVI for treating contaminated water.

Received 27th August 2020
Accepted 15th October 2020

DOI: 10.1039/d0em00375a

rsc.li/espi

Environmental significance

Sulfidation of nZVI with lower-valent sulfur can enhance the electron efficiency and selectivity of nZVI towards target contaminants. A conventional sulfidation process is generally carried out in an aqueous solution with an unstable reducing sulfur agent such as Na_2S and $Na_2S_2O_4$, which may result in the consumption of active Fe^0 and emission of toxic H_2S. To avoid these problems, we develop a new method where nZVI is sulfidated in ethanol with stable, non-toxic and easily available S^0 as the sulfidation agent. This is the first report on the chemical synthesis of S-nZVI using solid S^0. It provides a new way to use S^0 as an industrial byproduct for the large-scale application of S-nZVI in the remediation of contaminated sites.

1. Introduction

Nanoscale zero valent iron (nZVI) has great potential for the treatment of a spectrum of toxic and harmful environmental contaminants, specially halogenated persistent organic pollutants.[1–3] However, the reaction of nZVI with natural oxidative species, such as O_2 and H_2O/H^+, can accelerate the surface passivation of nZVI and decrease its treatment capacity for

[a]State Key Laboratory of Organic Geochemistry, Guangdong Provincial Key Laboratory of Environmental Protection and Resources and Utilization, Guangdong-Hong Kong-Maco Joint Laboratory for Environmental Pollution and Control, Guangzhou Institute of Geochemistry, Chinese Academy of Sciences, Guangzhou 510640, China. E-mail: zhongyin@gig.ac.cn; Fax: +86-20-85290117; Tel: +86-20-85290142

[b]University of Chinese Academy of Sciences, Beijing 100049, China

[c]Department of Environmental Sciences, Rutgers, The State University of New Jersey, 14 College Farm Road, New Brunswick, NJ 08901, USA

[d]School of Environment and Civil Engineering, Dongguan University of Technology, Dongguan 523808, China

[e]Guangdong Key Laboratory of Contaminated Sites Environmental Management and Remediation, Guangdong Provincial Academy of Environmental Science, Guangzhou 510045, China

† Electronic supplementary information (ESI) available: Details on additional information on materials, SEM and TEM images, SEM and EDS spectra, Fe 2p and S 2p XPS spectra, BET specific surface area, hydrodynamic diameter, zeta potential of $S\text{-nZVI}^S$ with different extents of sulfidation, HER kinetics model and model parameters, primary debromination pathway of TBBPA by nZVI and $S\text{-nZVI}^S$, product distribution, theoretical and actual S/Fe of $S\text{-nZVI}^S$ with different sulfur doses and electrochemical characterization results of the modified GCE with S-nZVI with different extents of sulfidation, and the transformation of TBBPA by $S\text{-nZVI}^{Na_2S}$ and $S\text{-nZVI}^{Na_2S_2O_4}$. See DOI: 10.1039/d0em00375a

target contaminants.[4,5] Recent studies have shown that the modification of nZVI with reducing sulfur compounds (S-nZVI) has greater advantages over original nZVI because S-nZVI can inhibit the H_2 evolution reaction (HER, reduction of water by Fe^0 to form hydrogen), increase the electron efficiency and selectivity for dehalogenation, and achieve more efficient long-term performance.[6–11]

Laboratory methods currently available for the sulfidation of nZVI include one-pot and two-pot methods.[12] For the one-pot method (aqueous–aqueous sulfidation), a solution mixture of sodium borohydride ($NaBH_4$) and sodium dithionite ($Na_2S_2O_4$) is simultaneously added into an Fe^{2+}/Fe^{3+} solution to produce S-nZVI particles.[13] In the two-pot method (aqueous-solid sulfidation), nZVI is firstly synthesized using the reduction of Fe^{2+}/Fe^{3+} solution by $NaBH_4$, and subsequently sulfidated with commonly used sulfidation agents such as sodium sulfide (Na_2S), $Na_2S_2O_4$ or sodium hyposulfite ($Na_2S_2O_3$) solutions.[10,14] These conventional sulfidation methods carried out in aqueous solutions with unstable reducing sulfur agents may suffer from some limitations, including (1) a large part of Fe^0 can be oxidized by high-valent sulfur species (*e.g.* $S_2O_4^{2-}$), causing the consumption of active Fe^0; (2) toxic and harmful H_2S can be released during sulfidation processes; (3) active Fe^0 reacts with water to cause the loss of reduction capacity of the synthesized particles.[15] It is important to use safe and stable sulfidation agents to develop environmentally friendly sulfidation technologies for the large-scale application of S-nZVI in environmental remediation.

Elemental sulfur (S^0) is considered as an inexpensive, stable and non-toxic sulfur agent under normal conditions.[15] It is easily available and mainly produced as a by-product or waste in oil refineries, gas processors, metal smelters, and coal/oil burning electric power plants.[16] The application of S^0 as an industrial byproduct in environmental remediation has received extensive attention. S^0 can be used as an electron donor for autotrophic denitrification in the biological treatment of nitrate contaminated water and microbial reduction of chromium(VI), vanadium(V) and perchlorate from contaminated aquifers.[17–20] Recently, Gu *et al.*[15] have synthesized sulfidated microscale ZVI (S-mZVI) by ball-milling solid microscale ZVI and S^0 powder. The ball-milling method allows the contact between S^0 and Fe^0 to form an Fe/FeS composite. Nevertheless, the ball-milling method is generally applied for the grinding of microscale ZVI into nZVI rather than for milling of nZVI. Until now, no information is available on the sulfidation of nZVI with S^0.

The goal of this study is to develop an efficient chemical synthesis method of S-nZVI with S^0 as a sulfidation agent. Because solid nZVI cannot directly react with solid S^0, the first step of synthesis is to dissolve S^0 to increase the contact between nZVI and S^0. It is well known that S^0 is slightly dissolved in organic solvents rather than in water. Meryer[21] reported that the solubility of S^0 in ethanol, acetone, and hexane is 0.066, 2.7 and 0.25 wt% (g S/100 g solvent), respectively. Nevertheless, our preliminary experiment shows that nZVI only disperses well in ethanol. Previous studies have reported that ethanol is widely used in the synthesis process of nZVI particles, which can disperse and stabilize nZVI nanoparticles and protect nZVI from oxidation.[22,23] nZVI synthesized in ethanol solution exhibits greater capability to reductively transform pollutants compared to nZVI synthesized in aqueous solution.[23]

In this study, we successfully synthesized sulfidated nZVI particles (S-nZVI^S) by sulfidation of nZVI with S^0 dissolved in ethanol under mild conditions. The resulting S-nZVI^S was characterized for their surface properties, including the morphology, particle size, specific surface area, zeta potential, corrosion rate of surface Fe^0 in water, and electrochemical properties. They were also evaluated for their reductive capability using tetrabromobisphenol A (TBBPA) as the probing solute. TBBPA is a known flame retardant commonly used in printed circuit boards and as an additive flame retardant in polymers. Due to its extensive use, TBBPA has a high detection rate in wastewater and surface and underground water.[24–26] It has potential persistent organic pollutant properties and poses adverse effects on human health.[27,28] Previous studies reported that the conventional S-nZVI (prepared in aqueous solutions of $Na_2S_2O_4$ or Na_2S) had the potential for transforming TBBPA into less brominated products, like tribromobisphenol A (tri-BBPA), dibromobisphenol A (di-BBPA), monobromobisphenol A (mono-BBPA) and bisphenol A (BPA).[29,30] A comparison of reactivity towards TBBPA between S-nZVI^S and conventional S-nZVI prepared from Na_2S or $Na_2S_2O_4$ was conducted. In addition, the application of S-nZVI^S in the treatment of TBBPA-spiked environmental water samples (including river water, groundwater, and tap water) was also evaluated.

2. Materials and methods

Unless otherwise mentioned, all experimental work was carried out in anaerobic glove boxes (99.999% N_2, Super 1220/750, Mikrouna Co. Ltd., Shanghai, China). All aqueous solutions were made from ultrapure water (18.2 MΩ cm resistivity, unique multi-functional ultrapure water system). All liquids (*i.e.*, ultrapure water and ethanol) were deoxidized with N_2 for 40 min before being transferred to the anaerobic glove boxes and used in experiments. Details with respect to the chemicals used are provided in Text S1 in the ESI.†

2.1 Synthesis

The synthesis of nZVI was carried out in 500 mL vials according to the method described by Li *et al.*[29] Briefly, 180 mL of 0.3 M $NaBH_4$ aqueous solution was added dropwise to 60 mL of 0.2 M $FeCl_2 \cdot 4H_2O$ aqueous solution at a rate of 3 mL min^{-1}. After stirring for 15 min on a magnetic stirrer, the resulting nZVI particles were collected and rinsed using deoxygenated water and ethanol three times each. The obtained nZVI particles were used for the synthesis of sulfidated nZVI or for the subsequent degradation experiments.

S-nZVI^S was synthesized by sulfidation of nZVI with elemental sulfur (S^0) in ethanol. Firstly, the freshly prepared nZVI particles (~12 mmol) were added into 420 mL deoxygenated ethanol solution and dispersed by agitation with a magnetic stirrer to obtain nZVI suspensions. The nZVI

particles were not adsorbed onto the magnetic stirrer during the strong stirring at 800 rpm. Then, S^0 powder was added to the ethanol suspension of nZVI, and the mixture was stirred for 12 h on a magnetic stirrer at 800 rpm to allow equilibration. After equilibration, the resulting S-nZVI^S suspensions were collected and rinsed using deoxygenated water and ethanol three times each. The amount of S^0 added into ethanol varied from 0.18 to 3.0 mmol to achieve theoretical S/Fe molar ratios ranging from 0.015 to 0.25. The solubility of S^0 in ethanol is 0.066 wt% (g S/100 g solvent). It means that 6.84 mmol S^0 can be dissolved in 420 mL ethanol. Therefore, it can be expected that 0.18–3.0 mmol of S^0 can be completely dissolved in ethanol.

Two types of conventional sulfidated nZVI particles were synthesized. One is Na_2S-sulfidated nZVI, denoted as S-nZVI^{Na_2S}, which was prepared by sonicating in an aqueous suspension of nZVI with 0.0012–0.04 M Na_2S for 40 min to obtain S-nZVI^{Na_2S} at a S/Fe ratio of 0.015–0.5 according to the two-pot method described by Rajajayavel and Ghoshal.[10] The other is $Na_2S_2O_4$-sulfidated nZVI (denoted as S-nZVI^{Na_2S_2O_4}) synthesized *via* the dropwise addition of 180 mL of mixed 0.3 M $NaBH_4$ and 0.0005–0.025 M $Na_2S_2O_4$ solution into 60 mL of $FeCl_2$ solution to obtain S-nZVI^{Na_2S_2O_4} at a S/Fe ratio of 0.015–0.75 according to the one-pot method described by Li *et al.*[29]

2.2 Particle characterization

The morphology and elemental mapping of solid-phase mineral particles were observed using an ultra high resolution field emission scanning electron microscope equipped with an energy dispersive spectrometer (FE-SEM-EDS, Carl-Zeiss, Merlin, Germany) and a transmission electron microscope coupled with an energy dispersive X-ray spectroscopy (TEM-EDS; FEI Talos F200S). The near-surface composition and chemical states of the nanoparticles were analyzed by X-ray photoelectron spectroscopy using a monochromatic Al Kα X-ray source (XPS, Thermo Fisher VG Scientific, West Sussex, UK). The binding energies of the photoelectrons were calibrated with reference to the C 1s peak at 284.8 eV. To measure the specific surface area, the dry powder samples were determined using an ASAP 2020 instrument through the N_2-BET adsorption method (Micromeritics, Atlanta, USA). The particle sizes and zeta (ζ) potentials were measured by using a Zetasizer Nano-ZS90 (Malvern instruments Ltd., Worcs, UK).

2.3 H_2 production tests

The H_2 evolution of nZVI and S-nZVI^S was measured to determine the corrosion rate of nZVI and S-nZVI^S with water. At interval times, 2 mL of nitrogen was injected into the bottles and then 2 mL of headspace was withdrawn and introduced directly into a gas chromatograph for quantitative analysis. The H_2 quantification in the vial headspace was performed on a Gas Chromatograph (6890N, Agilent Technologies, USA) custom configured by Wasson ECE Instrumentation with capillary and packed columns, in conjunction with a thermal conductivity detector (GC-TCD).

2.4 Electrochemical analysis

The electrochemical analysis of nanoparticles was performed on a CHI660E electrochemical work station (Chenhua Instrument Co., Ltd. Shanghai, China) and an anaerobic three-electrode cell (Gaossunion photoelectric Technology Co., Ltd. Tianjin, China) containing a glassy carbon electrode (GCE) as the working electrode, a Pt wire counter electrode, and a saturated calomel reference electrode (SCE). All potentials were measured with respect to the SCE reference. The 0.1 M phosphate buffer solution (PBS, pH = 7), as the electrolyte, was deoxidized by purging nitrogen (99.999%) for 20 min prior to use.

Before using, the GCE was activated and prepared according to a method reported previously.[29] The well prepared bare GCE was modified with nZVI or S-nZVI^S in an anaerobic glovebox, and then inserted slowly into the deoxidized electrolyte and sealed immediately in a cell. In this study, Tafel curve analysis, cyclic voltammetry (CV), and electrochemical impedance spectroscopy (EIS) were successively applied to analyze the electrochemical properties of the nanoparticles. For each electrochemical analysis, GCEs were modified with the fresh materials in an anaerobic glovebox. The electrochemical analysis was generally carried out in a sequence that proceeds from EIS to CV followed by Tafel curve analysis.[31]

The Tafel polarization curve was obtained at a scanning speed of 10 mV s^{-1}, using a potential of ±300 mV with respect to the open circuit potential just measured. The CV experiments were performed in a potential range between −0.8 and 0.6 V at a scan rate of 0.1 V s^{-1} for 6 cycles. The reducing power of the nanoparticles was evaluated from the value of the standard redox potential (E^0), which can be given by the mid-point potential (E_{mid}) obtained from the average of anodic and cathodic peak potentials ($E_{p,a}$ and $E_{p,c}$) in cyclic voltammetry, as shown in eqn (1) and (2).[32,33]

$$E_{mid} = E^0 + (RT/nF)\ln(D_R/D_O)^{1/2} \quad (1)$$

$$E_{mid} = (E_{p,a} + E_{p,c})/2 \quad (2)$$

For EIS measurements, the open circuit potential (OCP) was firstly determined, and then EIS measurements were carried out at an amplitude of 0.005 V in the frequency range from 10^5 to 0.1 Hz. The obtained results were shown as a Nyquist plot: the imaginary (Z'') *vs.* real (Z') parts of the impedance. In the typical Nyquist plot, the semicircular region at high frequency represents the charge transfer resistance (R_{ct}) at the surface of the electrodes, and the diameter of the extrapolated semicircle can reflect the value of R_{ct}. The straight-line region at low frequency represents Warburg resistance, also known as mass transfer impedance.[34]

2.5 Debromination tests

The debromination experiment of TBBPA was conducted in 150 mL glass serum bottles capped with PTFE-lined silicone septa. Initially, a certain amount of nZVI, S-nZVI^S, S-nZVI^{Na_2S}, or S-nZVI^{Na_2S_2O_4} was added into 98 mL ultrapure water to obtain an aqueous suspension of 2.3 g L^{-1} of nZVI or S-nZVI, respectively. The reaction was initiated by adding 2 mL TBBPA stock solution (1000 mg L^{-1}, deoxygenated methanol) into the suspension to achieve a final concentration of 20 mg L^{-1}. The reactors were

placed on a magnetic stirrer at 800 rpm at room temperature (30 ± 1 °C). At determined intervals, an aliquot of 2 mL of reaction suspension was sampled for the determination of the residual concentration of TBBPA and its debromination products (*i.e.*, tri-BBPA, di-BBPA, mono-BBPA and BPA). A control experiment without nZVI or S-nZVI^S particles was carried out and no TBBPA loss occurred.

In order to evaluate the potential of applying S-nZVI^S in the real water matrix, the efficiency of debromination of TBBPA in river, ground and tap water was determined. Different real water samples were used, including river water (collected from the Pearl River in Guangdong Province, South China), groundwater (collected from a well at the Guangzhou institute of Geochemistry, Chinese academy of science), and tap water (collected from the laboratory). Prior to use, the natural water samples were filtered with a 0.45 μm membrane and diluted ten times. The experimental procedures are similar to those mentioned above, except that a lower initial concentration of TBBPA (5 mg L^{-1}) is used to stimulate the real contaminated environments.[35]

The residual concentration of TBBPA and its debromination products in the samples were determined according to the method described by Li *et al.*[29] Briefly, 2 mL samples were dissolved by adding ~0.1 mL of 5 M HCl to facilitate the liberation of adsorbed TBBPA from solids. Subsequently, 2 mL methanol was added into each sample and mixed vigorously on a vortex mixer. Finally, a 1 mL aliquot was sampled for the analysis of TBBPA and its debromination products by using a HPLC-UV system (Shimadzu LC-20A, Kyoto, Japan) with the UV detection wavelength set at 210 nm. An Agilent ZORBAX Eclipse Plus C18 reversed-phase column (250 × 4.6 mm, 5 μm particle size; Agilent, Santa Clara, USA) was employed for the separation. The mobile phase was composed of 80% methanol and 20% water (containing 0.2% acetic acid) at a constant flow rate of 1.0 mL min^{-1}. The sample injection volume was 20 μL.

3. Results and discussion

3.1 Morphology and structure of S-nZVI^S

The morphologies and structures of S-nZVI^S were investigated by SEM-EDS and TEM in conjunction with elemental mapping of Fe, O and S (Fig. 1, S1 and S2†). Compared to original nZVI particles, S-nZVI^S had a similar chain-like structure but formed through the connection of smaller spherical particles in the size range of 50–100 nm (Fig. 1). These small spherical particles exhibited a core–shell structure, which is similar to that of S-nZVI particles obtained from the aqueous-solid sulfidation method with Na_2S.[36] Studies indicate that the sulfur dose can lead to different morphologies of S-nZVI. A high sulfur dose (S/Fe ratio > 0.1) results in a hollow structure formed in a process analogous to the Kirkendall effect[36] or flake-like structure formed from the precipitation of secondary iron sulfides on the nZVI surface.[37] In this study, however, a high sulfur dose (S/Fe ratio = 0.25) still preserved the chain-like and the core–shell structure of the original nZVI (Fig. 1, S1 and S3†). It is likely due to the fact that different synthesis processes yielded different surface functional groups that may affect the morphologies of the synthesized S-nZVI particles.[36]

The elemental mapping of the S-nZVI^S surface by TEM showed that Fe and S elements were highly dispersed on the surface of the S-nZVI^S particles (Fig. 1). The composition and chemical state of Fe and S on the surface of S-nZVI^S particles were identified by XPS analysis (Fig. 2, S4 and S5, Table S1†). The S(2p) spectra of S-nZVI^S showed two peaks (Fig. 2A and S4†). One is at a binding energy (B.E.) of 161.4 ± 0.2 eV (corresponding to S^{2-} species), and the other is the contribution at

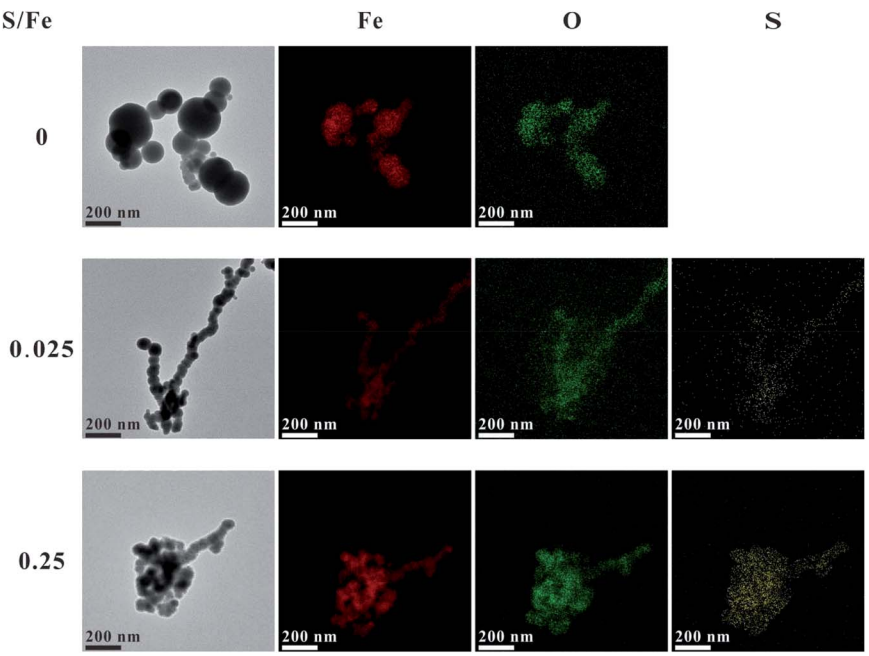

Fig. 1 TEM images and elemental mappings of Fe, O and S of S-nZVI^S at different S/Fe molar ratios.

162.6 ± 0.1 eV (corresponding to S_2^{2-} species), suggesting that S^0 was reduced to S^{2-} and S_2^{2-}. As shown in Fig. 2C, D and S5,† the Fe $2p_{3/2}$ spectra of nZVI are dominant by Fe^0 (B.E. = ~706.5 eV), Fe(II)–O (B.E. = ~710.1 eV), and Fe(III)–O (B.E. = ~713.4 eV). For the Fe $2p_{3/2}$ spectra of S-nZVI^S, however, the relative abundance of Fe(II)–O and Fe(III)–O decreased significantly and the Fe^0 peak was shifted to the peak at a B.E. of ~706.7 eV corresponding to Fe^0/Fe(II)–S.[37] Furthermore, the Fe(II)–S peak at a binding energy near 707.4 eV increased (Fig. 3D),[38] providing direct evidence that Fe^0 could directly react with S^0 dissolved in ethanol to form iron sulfides. It indicates that nZVI can be sulfidated successfully with S^0 dissolved in ethanol under mild conditions. The reactions between Fe^0 and S^0 dissolved in ethanol are proposed and described by eqn (3) and (4). The reaction mechanisms have been reported in the ball-milling of Fe^0 and S^0,[39] and the preparation of S-nZVI from $Na_2S_2O_4$ using one-pot synthesis.[40,41]

$$Fe^0 + S^0_{ethanol} = FeS \quad (3)$$

$$FeS + S^0_{ethanol} = FeS_2 \quad (4)$$

Fig. 2B demonstrates that the abundance of S^{2-} and S_2^{2-} species increased with an increase in the S/Fe ratio, which was consistent with the results of EDS analysis that the atomic ratio of S increased with an increase in the theoretical S/Fe ratio (Fig. S2 and Table S2†). The actual S doping amount was close to that introduced theoretically when the theoretical values of the S/Fe ratio were less than 0.025, revealing that the introduced S^0 was completely doped into nZVI in ethanol solution. When the theoretical values of S/Fe increased up to 0.05, 0.1, and 0.25, however, the atomic ratios of S/Fe on the surface of S-nZVI were only 0.038, 0.07 and 0.13, respectively, suggesting the incomplete incorporation of S into the surface of nZVI at a relatively higher S/Fe ratio. A similar phenomenon has been reported in prior studies for S-nZVI made from Na_2S[37] and S-mZVI made from S^0 using a two-pot approach.[15] The decrease in the S

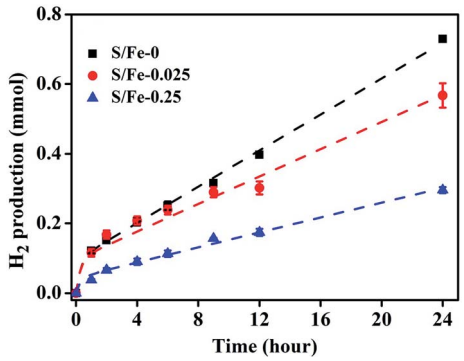

Fig. 3 H_2 evolution for S-nZVI^S at different S/Fe molar ratios and fit to the independent changes in the two reactive phase model (dashed curves). The initial concentration of S-nZVI^S is 2.3 g L^{-1} and the initial pH is 7.

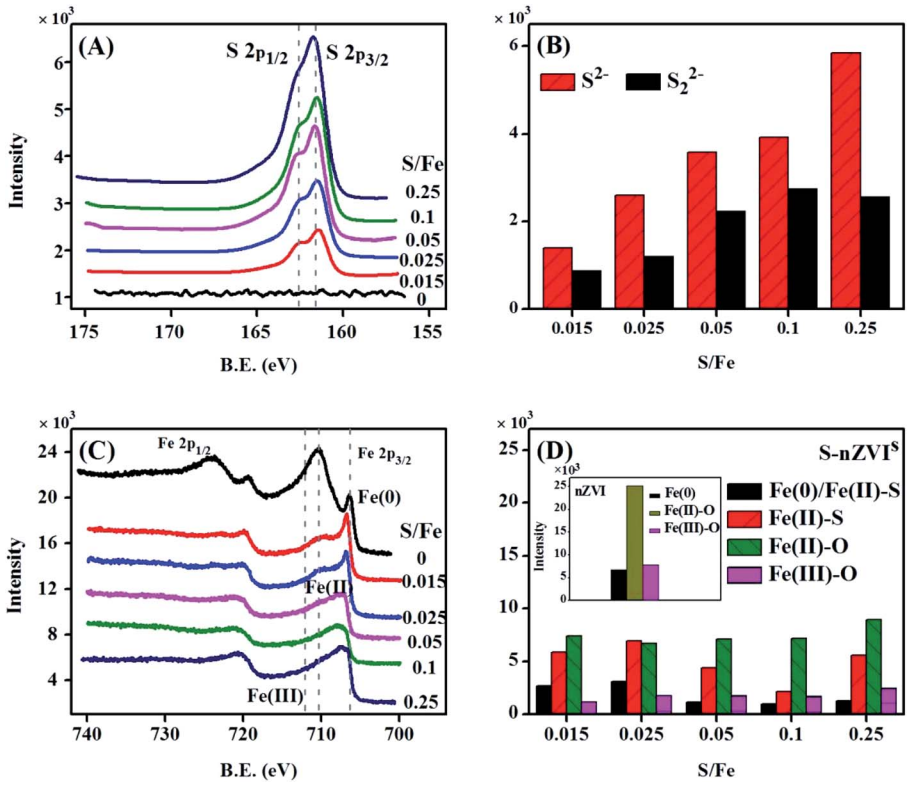

Fig. 2 XPS S 2p narrow region spectra (A), S species distribution (B), XPS Fe 2p narrow region spectra (C) and Fe species distribution (D) for S-nZVI^S at different S/Fe molar ratios.

uptake is likely caused by the decrease in available Fe surface sites due to the formation of iron sulfides.[37,42]

The effect of the S/Fe ratio on the hydrodynamic diameter, surface charge and specific surface areas of S-nZVI^S was investigated. The hydrodynamic diameter of S-nZVI^S measured by DLS was ~600 nm when the S/Fe molar ratio ranged from 0.015 to 0.05. As the S/Fe ratio increased up to 0.25, the hydrodynamic diameter significantly decreased to 109.3 ± 18.3 nm (Fig. S6A†). The decrease in the particle aggregation may be due to the deposition of more negatively charged iron sulfides on the nZVI surface.[15,43] As shown in Fig. S6B,† the zeta potential of S-nZVI^S increased with the extent of sulfidation. For example, the zeta potential of S-nZVI$^{S\text{-}0.25}$ was −44.8 ± 3.9 mV, which was 2.7 times higher than that of nZVI (−16.3 ± 2.0 mV). S-nZVI^S with a larger negative charge can enhance electric repulsion to prevent the particle aggregation.[10] This phenomenon has been extensively reported for sulfidated nZVI.[6,15] A decrease in particle aggregation could result in an increase in the particle specific surface area. The measured N_2-BET specific surface area of S-nZVI^S was increased with the sulfidation extent, which is consistent with prior studies (Fig. S6C†).[10]

3.2 H_2 evolution

The formation of H_2 from the reaction of Fe^0 with H_2O is an important process that controls the reactivity of nZVI in environmental media. It can cause corrosion of nZVI, the consumption of Fe^0 and thereby adversely affect the reduction of contaminants by nZVI. In order to evaluate the impact of sulfidation on the reactivity of nZVI, the HER from S-nZVI^S and nZVI was determined and the data were fit to four alternative kinetic models proposed by Qin *et al.*[44] As shown in Fig. 3 and S7† and Tables S3–S6,† the HER kinetics of S-nZVI^S and nZVI are described better with the independent changes in the two reactive phase model than the other three models (*i.e.*, first-order passivation of the Fe^0 model, replacement of the reactive phase model, and advanced phase replacement model), which is consistent with the result of study by Qin *et al.*[44] In the independent changes in the two reactive phase model (eqn (5)–(7)), the HER arises from a more reactive phase (phase 1, producing a fast stage) and a less reactive phase (phase 2, producing a slower stage), and they act independently. The faster stage of the HER may be attributed to the reactive mineral intermediate phase like ferrous oxyhydroxides formed on the nZVI surface during preparation, while the slower stage of the HER is caused by the reaction of Fe^0.

$$[H_2] = A \times (1 - e^{-k_1 t}) + B \times (1 - e^{-k_2 t}) \quad (5)$$

$$A = \frac{k_{H_2,1} \times S_{1,0}}{k_1} \quad (6)$$

$$B = \frac{k_{H_2,2} \times S_{2,0}}{k_2} \quad (7)$$

The fitting model parameters are shown in Tables S5.† The fitted values of A (*i.e.*, $k_{H_2,1} \times S_{1,0}/k_1$) and B (*i.e.*, $k_{H_2,2} \times S_{2,0}/k_2$) can be used to compare the effect of sulfidation on the HER

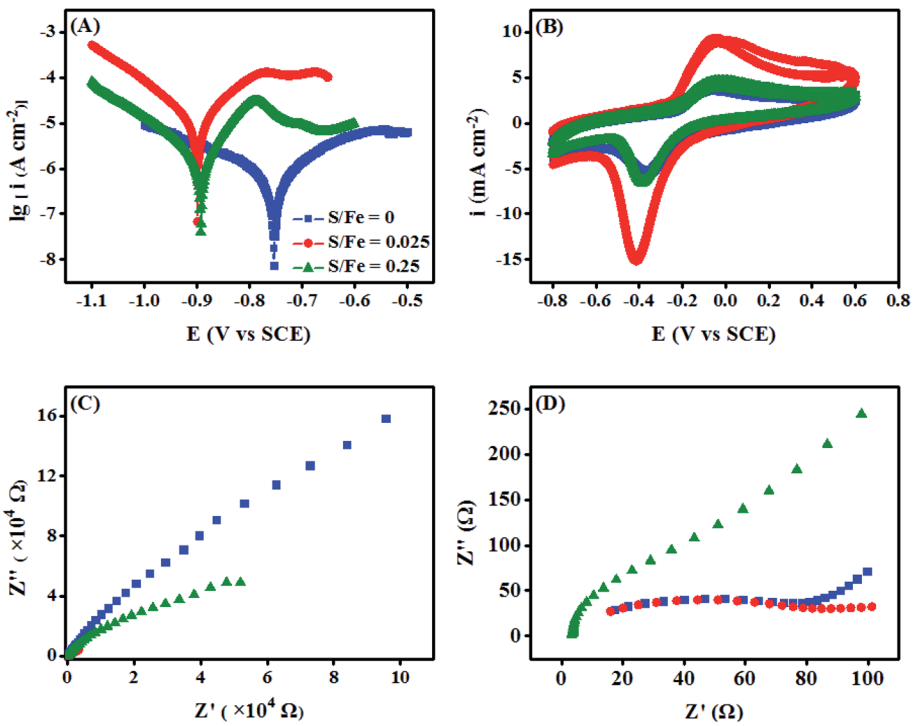

Fig. 4 Electrochemical characterization of the GCEs modified with S-nZVI^S at a S/Fe of 0, 0.025, or 0.25. (A) Tafel polarization curve, (B) cyclic voltammogram (CV) and (C) Nyquist profiles of electrochemical impedance spectroscopy (EIS) in the frequency range of 0.1 to 10^5 Hz; (D) Nyquist plot of electrochemical impedance spectroscopy (EIS) at high frequency.

kinetics. The values of A and B are higher and the HER is faster. It was observed that A values could be in the decreasing order of nZVI ≈ S-nZVI$^{S\text{-}0.025}$ > S-nZVI$^{S\text{-}0.25}$, while B values could be in the decreasing order of nZVI > S-nZVI$^{S\text{-}0.025}$ > S-nZVI$^{S\text{-}0.25}$, indicating that the sulfidation of nZVI with a higher dose of S^0 slowed the HER to a larger extent. The pH values in the reaction solution containing S-nZVI with or without TBBPA were lower than those for nZVI (Fig. S8†), further confirming that less OH^- was generated and the reduction rate of water was lower in the S-nZVI^S system than in the nZVI system. It is in agreement with the result of previous studies that the sulfidation of nano- and micro-ZVI can inhibit the HER.[10,15,41] The HER slowed by sulfidation with S^0 in ethanol may be attributed to two reasons: (1) sulfidation with S^0 in ethanol can decrease the generation of reactive ferrous oxyhydroxides, evidenced by the XPS analysis result that less Fe(II)–O was formed on S-nZVI^S than on nZVI; (2) iron sulfides formed are more hydrophobic than the iron oxides, slowing the corrosion of Fe^0 by water.[10,36,41]

3.3 Electrochemical characterization

The electrochemical characterization of S-nZVI^S and nZVI was performed using Tafel polarization curve analysis, cyclic voltammetry (CV), and electrochemical impedance spectroscopy (EIS) to evaluate the effect of sulfidation with S^0 in ethanol on the electron transfer behaviors. The Tafel curves analysis illustrated in Fig. 4A and Table S7† showed that sulfidation increased the corrosion rate and corrosion potentials (E_{corr}, more negative) of nZVI in water. Similarly, He *et al.*[7] found that the sulfidation of nZVI with Na_2S leads to an increase of corrosion current (I_{corr}) from 0.61 μA to 1.0 μA. Gu *et al.*[15] reported that the sulfidation of mZVI by ball-milling with S^0 favors more negative potentials. Turcio-Ortega *et al.*[45] demonstrated that Fe/FeS had more negative E_{corr} than Fe/FeO and supported greater charge transfer under various environmentally relevant solution conditions. S-nZVI$^{S\text{-}0.025}$ exhibited higher E_{corr} but lower HER than nZVI, suggesting that sulfidation increases the hydrophobicity of nZVI to inhibit the reaction between nZVI and water.[7,36,42] Noted that E_{corr} and I_{corr} did not continuously increase with the increase of the sulfidation extent. S-nZVI$^{S\text{-}0.25}$ had lower I_{corr} and less negative E_{corr} than S-nZVI$^{S\text{-}0.025}$. CV analysis also showed that the mid-point potential (E_{mid}) values were less negative for S-nZVI$^{S\text{-}0.25}$ (−213.5 mV) than that of S-nZVI$^{S\text{-}0.025}$ (−229.5 mV) (Fig. 4B, Table S8†). The EIS results shown in Fig. 4C and D suggested that S-nZVI$^{S\text{-}0.25}$ had a larger semicircle diameter and provided a higher electron transfer resistance (R_{ct}).[46] The trend for R_{ct} was in good agreement with that for polarization resistance (R_p) obtained from Tafel curves. The increased electron transfer resistance resulted in an inhibition in the electron transfer that suppressed H_2 formation from the reduction of water by S-nZVI$^{S\text{-}0.25}$ (Fig. 3).

3.4 Debromination of TBBPA by S-nZVI^S

As shown in Fig. 5A, TBBPA could be transformed rapidly by S-nZVI^S with a S/Fe ratio of 0.015–0.05 compared to nZVI. About 91.4% of TBBPA was transformed by S-nZVI$^{S\text{-}0.025}$ within 2 hours, which was 3 times higher than that of nZVI (28.8%). TBBPA transformation was well described by the pseudo-first-order rate model (Fig. S9†). The fitted rate constants for TBBPA removal (k_{obs}) are given in Table S9† and the corresponding surface area normalized reaction constants (k_{SA}) of TBBPA transformation are shown in Fig. 5B. The k_{SA} values were increased as the S/Fe ratio increased from 0.015 to 0.025. S-nZVI$^{S\text{-}0.025}$ had the highest transformation rate constant of TBBPA with a k_{SA} of 0.066 ± 0.0076 L h^{-1} m^{-2}. Previous studies reported that sulfidation can facilitate the electron transfer from Fe^0 to contaminants rather than natural reductants involving H_2O.[6,11,36] It is mainly due to the fact that sulfidation increases the hydrophobicity of nZVI to hinder the H adsorption but to enhance the adsorption of hydrophobic contaminants and therefore increase the electron selectivity.[36,42] S-nZVI$^{S\text{-}0.025}$ exhibited a higher transformation rate of TBBPA but a lower HER rate compared to nZVI, suggesting that the electron efficiency of TBBPA debromination of S-nZVI$^{S\text{-}0.025}$ may be higher than that of nZVI. S-nZVI$^{S\text{-}0.25}$ exhibited a lower reactivity with TBBPA than nZVI, which was mainly attributed to its larger electron transfer resistance, evidenced by EIS analysis. Nevertheless, the k_{SA} gradually decreased to 0 when the S/Fe ratio increased up to 0.25. It may be caused by the fact that FeS itself does not contribute to the TBBPA debromination[47] and the availability of active Fe^0 sites for TBBPA transformation is limited due to the presence of FeS.

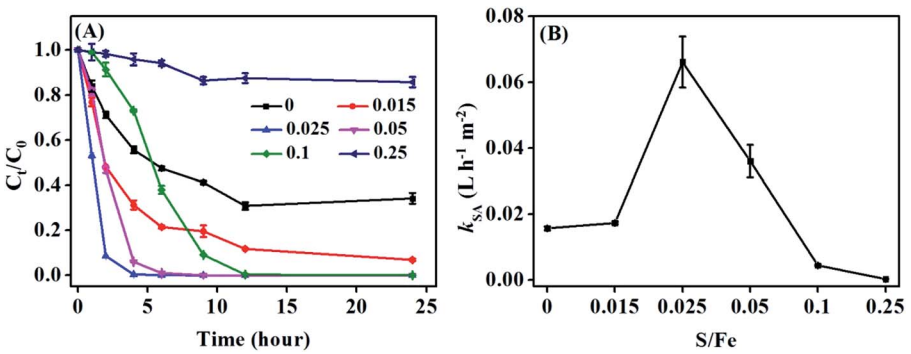

Fig. 5 Transformation of TBBPA by S-nZVI^S (A) and the surface area-based pseudo-first-order rate constant (k_{SA}) (B) of TBBPA transformation at different S/Fe molar ratios. The initial concentration of S-nZVI^S and TBBPA is 2.3 g L^{-1} and 20 mg L^{-1}, respectively.

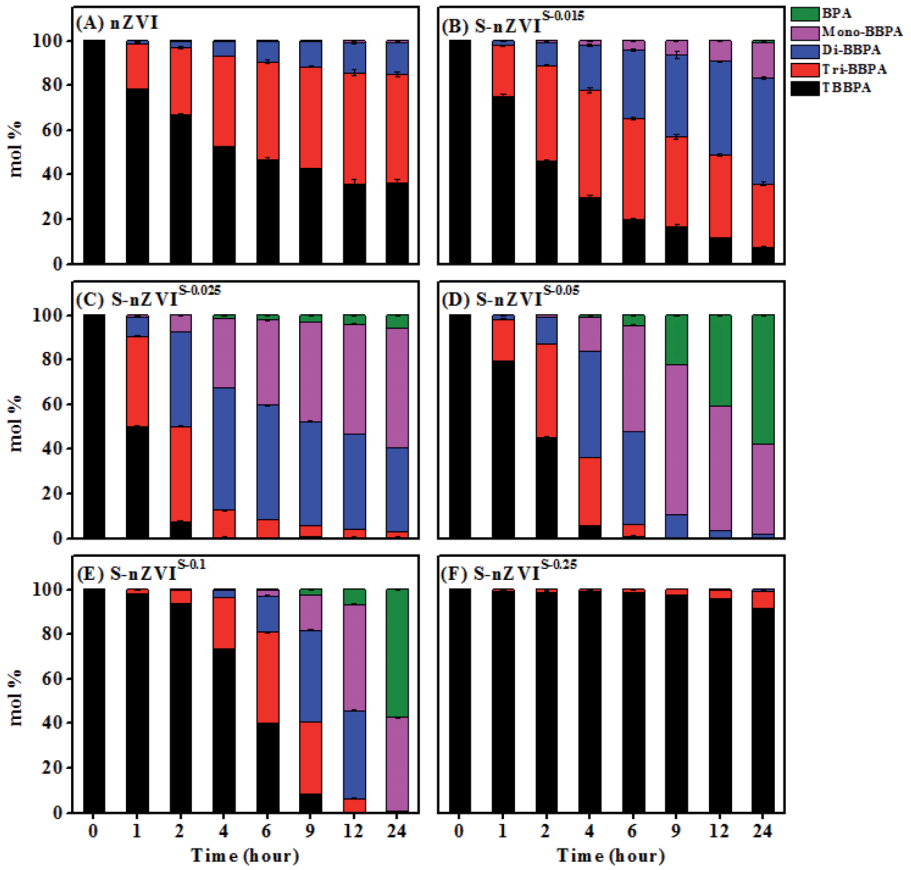

Fig. 6 Molar percentage of intermediate products during the transformation of TBBPA by S-nZVI^{S} at different S/Fe molar ratios. (A) nZVI, (B) S/Fe = 0.015, (C) S/Fe = 0.025, (D) S/Fe = 0.05, (E) S/Fe = 0.1, and (F) S/Fe = 0.25. The initial concentration of S-nZVI^{S} and TBBPA is 2.3 g L^{-1} and 20 mg L^{-1}, respectively.

Tri-BBPA, di-BBPA, mono-BBPA and BPA were produced in the TBBPA transformation by S-nZVI^{S} with a S/Fe ratio of 0.015–0.1 (Fig. 6). It is consistent with the result of S-nZVI obtained from one-pot synthesis with $Na_2S_2O_4$ and from the two-pot method with Na_2S,[29,30] in which TBBPA was transformed following a four-step sequential debromination pathway to form tri-BBPA, di-BBPA, mono-BBPA and BPA (Fig. S10†).[29] The amounts of the four intermediates varied with the sulfur loading during the reaction (Fig. 6). In the nonsulfidated nZVI system, tri- and di-BBPA were the dominant products and no BPA was detected. In contrast, BPA was formed and its concentration gradually increased with an increase in the degree of sulfidation. It may be resulted from the fact that iron sulfides with relatively greater hydrophobicity might be beneficial for the adsorption of intermediates onto the surface of S-nZVI and facilitate its degradation by Fe^0.[40] Nevertheless, S-nZVI with a S/Fe ratio of 0.25 only debrominated TBBPA into tri- and di-BBPA. It suggests that coating with a high dose of S prevents the debromination of TBBPA products by S-nZVI.

3.5 Comparison with S-nZVI^{Na_2S_2O_4} and S-nZVI^{Na_2S}

In order to compare the reactivity of S-nZVI^{S} towards TBBPA with that of conventional S-nZVI, the debromination rate of TBBPA by S-nZVI^{Na_2S_2O_4} and S-nZVI^{Na_2S} at different S/Fe ratios was also investigated (Fig. 7). For S-nZVI^{Na_2S_2O_4} particles, more than 95% TBBPA was removed at a high S/Fe ratio of 0.5–0.75 within 24 h of reaction, while only 8–30% removal of TBBPA was achieved at a low S/Fe ratio of 0.015–0.05. Different from S-nZVI^{Na_2S_2O_4} particles, S-nZVI^{Na_2S} exhibited higher reactivity towards TBBPA debromination at a low S/Fe ratio of 0.015–0.05. The highest TBBPA removal percentage of S-nZVI^{Na_2S} was 77.9% when the S/Fe molar ratio was 0.025. When the S/Fe molar ratio increased up to 0.5, the removal percentage of TBBPA by S-nZVI^{Na_2S} decreased to <10%. The TBBPA removal data of S-nZVI particles are also fitted well to the first-order rate kinetic model (Fig. S11†) and the rate constant values are shown in Table S9.† The highest k_{obs} value for S-nZVI^{Na_2S_2O_4} and S-nZVI^{Na_2S} was 0.38 $\pm$ 0.02 h^{-1} at a S/Fe ratio of 0.5 and 0.16 $\pm$ 0.018 h^{-1} at a S/Fe ratio of 0.025, respectively. Both of them were lower than 1.19 $\pm$ 0.071 h^{-1} for S-nZVI^{S} at a S/Fe ratio of 0.025. It suggests that S-nZVI made from S^0 dissolved in ethanol poses higher reactivity towards TBBPA than those conventional S-nZVI made from $Na_2S_2O_4$ and Na_2S dissolved in water. It may be attributed to the fact that sulfidation with S^0 in ethanol can protect Fe(0) from oxidation rather than in an aqueous phase. This could be confirmed by the XPS analysis result that S-nZVI^{S} had a higher relative abundance of Fe(0) and a lower relative abundance of Fe(II)–O/Fe(III)–O compared to S-nZVI^{Na_2S_2O_4} (Fig. S12A†). In

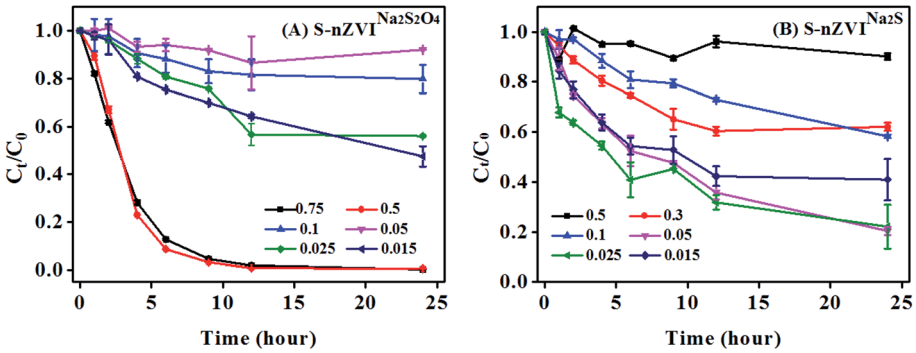

Fig. 7 Removal of TBBPA by S-nZVI^{Na_2S} and S-nZVI^{Na_2S_2O_4} with different S/Fe molar ratios. The initial concentration of S-nZVI^{S} and TBBPA is 2.3 g L^{-1} and 20 mg L^{-1}, respectively.

addition, the surface of S-nZVI^{S} was dominated by FeS and FeS_2, which were different from S^{2-} and S_n^{2-} distributed on the surface of S-nZVI^{Na_2S} and S-nZVI^{Na_2S_2O_4} (Fig. S12C and D†). Rajajayavel and Ghoshal[10] and Cao *et al.*[48] reported that different sulfide species on the nZVI surface can affect the reactivity of particles towards pollutants. Xu *et al.*[42] demonstrated that the FeS_2-like structure in S-nZVI makes the material surface more hydrophobic, facilitating a selective reaction with contaminants over water reduction.

3.6 Application of S-nZVI^{S} in the treatment of real water

For the purpose of assessing the potential performance of S-nZVI^{S} in real water, the removal of TBBPA in TBBPA-spiked real water (*i.e.*, the surface water from the Pearl River, groundwater, and tap water) was analyzed. As shown in Fig. 8, the unsulfidated nZVI has a small or negligible effect on the TBBPA removal, while S-nZVI^{S} significantly removed TBBPA from the contaminated water. The removal percentages of TBBPA reached 64.8 ± 0.4% in the Pearl River water, 52.63 ± 0.0% in groundwater, and 43.84 ± 2.3% in tap water within 24 h of reaction, respectively. The removal of TBBPA by S-nZVI$^{S\text{-}0.025}$ in the three real water samples fitted well with the pseudo-first-order kinetic model with a high correlation coefficient (Fig.-S13,†$R^2 > 0.98$). The pseudo-first-order rate constant for TBBPA removal was 0.047 ± 0.002 h^{-1} in Pearl River, 0.046 ± 0.002 h^{-1} in groundwater, and 0.037 ± 0.0008 h^{-1} in tap water. It suggests that S-nZVI$^{S\text{-}0.025}$ provides better performance than nZVI in the treatment of TBBPA-contaminated real water, which has great potential for the remediation of contaminated water.

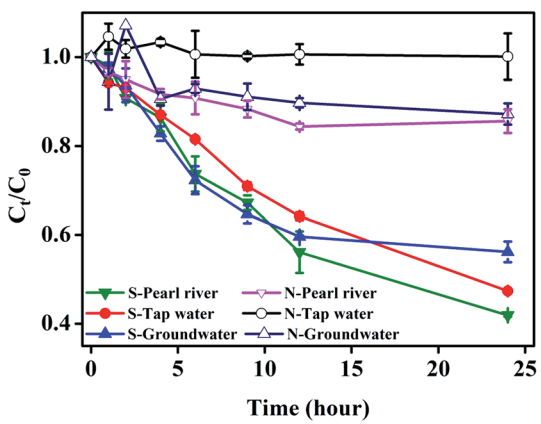

Fig. 8 Removal of TBBPA by nZVI (N-) and S-nZVI$^{S\text{-}0.025}$ (S-) from different real water samples. The initial concentration of S-nZVI particles and TBBPA is 2.3 g L^{-1} and 5 mg L^{-1}, respectively. The physical and chemical properties of the water samples are shown in Table S10.†

It should be noted that the removal rate of TBBPA by S-nZVI$^{S\text{-}0.025}$ in real water decreases 25–32 times compared to that in pure water, which may be caused by the complex aqueous chemical conditions of real water. The details on the analysis of aqueous chemical conditions of these real water samples, *e.g.*, pH, conductivity, biochemical oxygen demand (BOD_5), chemical oxygen demand (COD), and dissolved anions and cations, are provided in Table S10.† It was observed that the real water has higher conductivity, dissolved anion and cation concentrations and COD. It is well known that the reductive transformation of TBBPA contaminants by nZVI is a surface-mediated reaction, which is easily affected by various environmental conditions such as inorganic ions and organic compounds.[9,12,49] Competition for active sites between inorganic and organic compounds with TBBPA may result in a decrease in the transformation of TBBPA by nZVI. It is important to comprehensively understand the effects of these environmental factors on the removal of TBBPA by S-nZVI^{S}. In addition, the role of dissolved oxygen (O_2) in the transformation of TBBPA is deserved to be investigated as O_2 is widely distributed in the natural environments.[50,51] The obtained information will assist in the application of S-nZVI^{S} in site remediation under complex environmental conditions.

4. Conclusions

This study reports a novel chemical synthesis method of S-nZVI particles where nZVI is sulfidated with solid S^0 (an inexpensive, readily available and safe sulfidation agent) dissolved in ethanol under mild conditions. In the sulfidation process, a relatively homogeneous layer of FeS/FeS_2 is formed on the nZVI surface that can slow the corrosion reaction rate of Fe^0 and enhance the electron transfer. The resulting S-nZVI^{S} exhibited better

performance in TBBPA transformation than the conventional S-nZVI particles made from Na_2S and $Na_2S_2O_4$. The reactivity of S-nZVI^S towards TBBPA debromination is significantly affected by different S/Fe ratios. S-nZVI^S at a S/Fe ratio of 0.025 exhibited the best performance in the transformation of TBBPA and its debromination products, which has been successfully applied in the treatment of TBBPA-spiked real water. Taken together, this sulfidation method is safe, low-cost and easy to handle, which can be applied for removing halogenated organic contaminants from contaminated water.

Conflicts of interest

There are no conflicts to declare.

Acknowledgements

This study was supported financially by the National Natural Science Foundation of China (Grant Nos. 41773132 and 42077285), the Guangdong Foundation for Program of Science and Technology Research (Grant No. 2017B030314057 and 2019B121205006) and the State Key Laboratory of Organic Geochemistry, GIGCAS (Grant No. SKLOG-201910 and SKLOG2020-4). This is contribution No. IS-2925 from GIGCAS.

References

1 S. Bae, R. N. Collins, T. D. Waite and K. Hanna, Advances in surface passivation of nanoscale zerovalent iron (NZVI): A critical review,, *Environ. Sci. Technol.*, 2018, **52**, 12010–12025, DOI: 10.1021/acs.est.8b01734.

2 J. Du, J. Bao, C. Lu and D. Werner, Reductive sequestration of chromate by hierarchical FeS@Fe(0) particles, *Water Res.*, 2016, **102**, 73–81, DOI: 10.1016/j.watres.2016.06.009.

3 X. Zhao, W. Liu, Z. Cai, B. Han, T. Qian and D. Zhao, An overview of preparation and applications of stabilized zero-valent iron nanoparticles for soil and groundwater remediation, *Water Res.*, 2016, **100**, 245–266, DOI: 10.1016/j.watres.2016.05.019.

4 D. Fan, G. O. B. Johnson, P. G. Tratnyek and R. L. Johnson, Sulfidation of nano zerovalent iron (nZVI) for improved selectivity during *in situ* chemical reduction (ISCR), *Environ. Sci. Technol.*, 2016, **50**, 9558–9565, DOI: 10.1021/acs.est.6b02170.

5 Y. Sun, J. Li, T. Huang and X. H. Guan, The influences of iron characteristics, operating conditions and solution chemistry on contaminants removal by zero-valent iron: A review,, *Water Res.*, 2016, **100**, 277–295, DOI: 10.1016/j.watres.2016.05.031.

6 S. Bhattacharjee and S. Ghoshal, Optimal design of sulfidated nanoscale zerovalent iron for enhanced trichloroethene degradation, *Environ. Sci. Technol.*, 2018, **52**, 11078–11086, DOI: 10.1021/acs.est.8b02399.

7 F. He, Z. Li, S. Shi, W. Xu, H. Sheng, Y. Gu, Y. Jiang and B. Xi, Dechlorination of excess trichloroethene by bimetallic and sulfidated nanoscale zero-valent iron, *Environ. Sci. Technol.*, 2018, **52**, 8627–8637, DOI: 10.1021/acs.est.8b01735.

8 S. Huang, C. Xu, Q. Shao, Y. Wang, B. Zhang, B. Gao, W. Zhou and P. G. Tratnyek, Sulfide-modified zerovalent iron for enhanced antimonite sequestration: characterization, performance, and reaction mechanisms, *Chem. Eng. J.*, 2018, **338**, 539–547, DOI: 10.1016/j.cej.2018.01.033.

9 D. Li, X. Zhu, Y. Zhong, W. Huang and P. Peng, Abiotic transformation of hexabromocyclododecane by sulfidated nanoscale zerovalent iron: Kinetics, mechanism and influencing factors, *Water Res.*, 2017, **121**, 140–149, DOI: 10.1016/j.watres.2017.05.019.

10 S. R. Rajajayavel and S. Ghoshal, Enhanced reductive dechlorination of trichloroethylene by sulfidated nanoscale zerovalent iron, *Water Res.*, 2015, **78**, 144–153, DOI: 10.1016/j.watres.2015.04.009.

11 F. He, L. Gong, D. Fan, P. G. Tratnyek and G. V. Lowry, Quantifying the efficiency and selectivity of organohalide dechlorination by zerovalent iron, *Environ. Sci.: Processes Impacts*, 2020, **22**, 528–542, DOI: 10.1039/c9em00592g.

12 J. Li, X. Zhang, Y. Sun, L. Liang, B. Pan, W. Zhang and X. H. Guan, Advances in sulfidation of zerovalent iron for water decontamination, *Environ. Sci. Technol.*, 2017, **51**, 13533–13544, DOI: 10.1021/acs.est.7b02695.

13 E. J. Kim, J. H. Kim, A. M. Azad and Y. S. Chang, Facile synthesis and characterization of Fe/FeS nanoparticles for environmental applications, *ACS Appl. Mater. Interfaces*, 2011, **3**, 1457–1462, DOI: 10.1021/am200016v.

14 D. M. Fan, Y. Lan, P. G. Tratnyek, R. L. Johnson, J. Filip, D. M. O'Carroll, A. N. Garcia and A. Agrawal, Sulfidation of iron-based materials: a review of processes and implications for water treatment and remediation, *Environ. Sci. Technol.*, 2017, **51**, 13070–13085, DOI: 10.1021/acs.est.7b04177.

15 Y. Gu, B. Wang, F. He, M. J. Bradley and P. G. Tratnyek, Mechanochemically sulfidated microscale zero valent iron: Pathways, kinetics, mechanism, and efficiency of trichloroethylene dechlorination, *Environ. Sci. Technol.*, 2017, **51**, 12653–12662, DOI: 10.1021/acs.est.7b03604.

16 Y. Wang, C. Bott and R. Nerenberg, Sulfur-based denitrification: Effect of biofilm development on denitrification fluxes, *Water Res.*, 2016, **100**, 184–193, DOI: 10.1016/j.watres.2016.05.020.

17 R. Li, C. P. Feng, W. E. Hu, B. D. Xi, N. Chen, B. W. Zhao, Y. Liu, C. B. Hao and J. Y. Pu, Woodchip-sulfur based heterotrophic and autotrophic denitrification (WSHAD) process for nitrate contaminated water remediation, *Water Res.*, 2016, **89**, 171–179, DOI: 10.1016/j.watres.2015.11.044.

18 E. Sahinkaya and A. Kilic, Heterotrophic and elemental-sulfur-based autotrophic denitrification processes for simultaneous nitrate and Cr(VI) reduction, *Water Res.*, 2014, **50**, 278–286, DOI: 10.1016/j.watres.2013.12.005.

19 C. H. Shi, Y. L. Cui, J. P. Lu and B. G. Zhang, Sulfur-based autotrophic biosystem for efficient vanadium (V) and chromium(VI) reductions in groundwater, *Chem. Eng. J.*, 2020, **395**, 124972, DOI: 10.1016/j.cej.2020.124972.

20 D. J. Wan, Q. Li, Y. D. Liu, S. H. Xiao and H. J. Wang, Simultaneous reduction of perchlorate and nitrate in a combined heterotrophic-sulfur-autotrophic system:

Secondary pollution control, pH balance and microbial community analysis, *Water Res.*, 2019, **165**, 115004, DOI: 10.1016/j.watres.2019.115004.

21 B. Meyer, Elemental sulfur, *Chem. Rev.*, 1976, **76**, 367–388, DOI: 10.1021/cr60301a003.

22 S. M. Ponder, J. G. Darab and T. E. Mallouk, Remediation of Cr(VI) and Pb(II) aqueous solutions using supported, nanoscale zero-valent iron, *Environ. Sci. Technol.*, 2000, **34**, 2564–2569, DOI: 10.1021/es9911420.

23 Q. Wang, S. Snyder, J. Kim and H. Choi, Aqueous ethanol modified nanoscale zerovalent iron in bromate reduction: Synthesis, characterization, and reactivity, *Environ. Sci. Technol.*, 2009, **43**, 3292–3299, DOI: 10.1021/es803540b.

24 U. J. Kim and J. E. Oh, Tetrabromobisphenol A and hexabromocyclododecane flame retardants in infant-mother paired serum samples, and their relationships with thyroid hormones and environmental factors, *Environ. Pollut.*, 2014, **184**, 193–200, DOI: 10.1016/j.envpol.2013.08.034.

25 K. Liu, J. Li, S. Yan, W. Zhang, Y. Li and D. Han, A review of status of tetrabromobisphenol A (TBBPA) in China,, *Chemosphere*, 2016, **148**, 8–20, DOI: 10.1016/j.chemosphere.2016.01.023.

26 T. Malkoske, Y. Tang, W. Xu, S. Yu and H. Wang, A review of the environmental distribution, fate, and control of tetrabromobisphenol A released from sources,, *Sci. Total Environ.*, 2016, **569–570**, 1608–1617, DOI: 10.1016/j.scitotenv.2016.06.062.

27 A. Ballesteros-Gómez, J. Ballesteros, X. Ortiz, W. Jonker, R. Helmus, K. J. Jobst, J. R. Parsons and E. J. Reiner, Identification of novel brominated compounds in flame retarded plastics containing TBBPA by combining isotope pattern and mass defect cluster analysis, *Environ. Sci. Technol.*, 2017, **51**, 1518–1526, DOI: 10.1021/acs.est.6b03294.

28 N. Y. Yin, S. J. Liang, S. X. Liang, R. J. Yang, B. W. Hu, Z. F. Qin, A. F. Liu and F. Faiola, TBBPA and its alternatives disturb the early stages of neural development by interfering with the NOTCH and WNT pathways, *Environ. Sci. Technol.*, 2018, **52**, 5459–5468, DOI: 10.1021/acs.est.8b00414.

29 D. Li, Z. Mao, Y. Zhong, W. L. Huang, Y. D. Wu and P. A. Peng, Reductive transformation of tetrabromobisphenol A by sulfidated nano zerovalent iron, *Water Res.*, 2016, **103**, 1–9, DOI: 10.1016/j.watres.2016.07.003.

30 J. Wu, J. Zhao, J. Hou, R. J. Zeng and B. Xing, Degradation of tetrabromobisphenol A by sulfidated nanoscale zerovalent iron in a dynamic two-step anoxic/oxic process, *Environ. Sci. Technol.*, 2019, **53**, 8105–8114, DOI: 10.1021/acs.est.8b06834.

31 E. Kim, J. Kim, Y. Chang, D. Turcioortega and P. G. Tratnyek, Effects of metal ions on the reactivity and corrosion electrochemistry of Fe/FeS nanoparticles, *Environ. Sci. Technol.*, 2014, **48**, 4002–4011, DOI: 10.1021/es405622d.

32 P. A. Kilmartin, H. L. Zou and A. L. Waterhouse, A cyclic voltammetry method suitable for characterizing antioxidant properties of wine and wine phenolics,, *J. Agric. Food Chem.*, 2001, **49**, 1957–1965, DOI: 10.1021/jf001044u.

33 J. Heinze, Cycle voltammetry - electrochemical spectroscopy, *Angew. Chem., Int. Ed.*, 1984, **23**, 831–847, DOI: 10.1002/anie.198408313.

34 L. Wang, E. W. Diau, M. Wu, H. P. Lu and T. Ma, Highly efficient catalysts for Co(II/III) redox couples in dye-sensitized solar cells, *Chem. Commun.*, 2012, **48**, 2600–2602, DOI: 10.1039/c2cc1749a.

35 H. Li, M. J. La Guardia, H. Liu, R. C. Hale, T. M. Mainor, E. Harvey, G. Y. Sheng, J. M. Fu and P. A. Peng, Brominated and organophosphate flame retardants along a sediment transect encompassing the Guiyu, China e-waste recycling zone, *Sci. Total Environ.*, 2019, **646**, 58–67, DOI: 10.1016/j.scitotenv.2018.07.276.

36 J. Xu, Y. Wang, C. Weng, W. Bai, Y. Jiao, R. Kaegi and G. V. Lowry, Reactivity, selectivity, and long-term performance of sulfidized nanoscale zerovalent iron with different properties, *Environ. Sci. Technol.*, 2019, **53**, 5936–5945, DOI: 10.1021/acs.est.9b00511.

37 D. Fan, R. P. Anitori, B. M. Tebo, P. G. Tratnyek, J. S. Lezama Pacheco, R. K. Kukkadapu, M. H. Engelhard, M. E. Bowden, L. Kovarik and B. W. Arey, Reductive sequestration of pertechnetate ($^{99}TcO_4^-$) by nano zerovalent iron (nZVI) transformed by abiotic sulfide, *Environ. Sci. Technol.*, 2013, **47**, 5302–5310, DOI: 10.1021/es304829z.

38 H. Y. Jeong, Y. S. Han, S. W. Park and K. F. Hayes, Aerobic oxidation of mackinawite (FeS) and its environmental implication for arsenic mobilization, *Geochim. Cosmochim. Acta*, 2010, **74**, 3182–3198, DOI: 10.1016/j.gca.2010.03.012.

39 J. Z. Jiang, R. K. Larsen, R. Lin, S. Morup, I. Chorkendorff, K. Nielsen, K. Hansen and K. West, Mechanochemical Synthesis of Fe–S Materials, *J. Solid State Chem.*, 1998, **138**, 114–125, DOI: 10.1006/jssc.1998.7761.

40 M. Mangayayam, K. Dideriksen, M. Ceccato and D. J. Tobler, The structure of sulfidized zero-valent iron by one-pot synthesis: Impact on contaminant selectivity and long-term performance,, *Environ. Sci. Technol.*, 2019, **53**, 4389–4396, DOI: 10.1021/acs.est.8b06480.

41 Y. Han and W. Yan, Reductive dechlorination of trichloroethene by zero-valent iron nanoparticles: Reactivity enhancement through sulfidation treatment, *Environ. Sci. Technol.*, 2016, **50**, 12992–13001, DOI: 10.1021/acs.est.6b03997.

42 J. Xu, A. Avellan, H. Li, X. Liu, V. Noel, Z. Lou, Y. Wang, R. Kaegi, G. Henkelman and G. V. Lowry, Sulfur loading and speciation control the hydrophobicity, electron transfer, reactivity, and selectivity of sulfidized nanoscale zerovalent iron, *Adv. Mater.*, 2020, **32**, 1906910, DOI: 10.1002/adma.201906910.

43 E. J. Kim, K. Murugesan, J. H. Kim, P. G. Tratnyek and Y. S. Chang, Remediation of trichloroethylene by FeS-coated iron nanoparticles in simulated and real groundwater: Effects of water chemistry, *Ind. Eng. Chem. Res.*, 2013, **52**, 9343–9350, DOI: 10.1021/ie400165a.

44 H. Qin, X. H. Guan, J. Z. Bandstra, R. L. Johnson and P. G. Tratnyek, Modeling the kinetics of hydrogen

formation by zerovalent iron: Effects of sulfidation on micro- and nano-scale particles, *Environ. Sci. Technol.*, 2018, **52**, 13887–13896, DOI: 10.1021/acs.est.8b04436.

45 D. Turcio-ortega, D. Fan, P. G. Tratnyek, E. Kim and Y. Chang, Reactivity of Fe/FeS nanoparticles: Electrolyte composition effects on corrosion electrochemistry, *Environ. Sci. Technol.*, 2012, **46**, 12484–12492, DOI: 10.1021/es303422w.

46 F. B. Li, L. Tao, C. H. Feng, X. Z. Li and K. W. Sun, Electrochemical evidences for promoted interfacial reactions: The role of Fe(II) adsorbed onto gamma-Al_2O_3 and TiO_2 in reductive transformation of 2-nitrophenol,, *Environ. Sci. Technol.*, 2009, **43**, 3656–3661, DOI: 10.1021/es8033445.

47 D. Li, P. A. Peng, Z. Q. Yu, W. L. Huang and Y. Zhong, Reductive transformation of hexabromocyclododecane (HBCD) by FeS, *Water Res.*, 2016, **101**, 195–202, DOI: 10.1016/j.watres.2016.05.066.

48 Z. Cao, X. Liu, J. Xu, J. Zhang, Y. Yang, J. Zhou, X. Xu and G. V. Lowry, Removal of antibiotic florfenicol by sulfide-modified nanoscale zero-valent iron, *Environ. Sci. Technol.*, 2017, **51**, 11269–11277, DOI: 10.1021/acs.est.7b02480.

49 Y. Xie and D. M. Cwiertny, Use of dithionite to extend the reactive lifetime of nanoscale zero-valent iron treatment systems, *Environ. Sci. Technol.*, 2010, **44**, 8649–8655, DOI: 10.1021/es102451t.

50 Y. J. Yu, Z. Huang, D. Y. Deng, Y. M. Ju, L. Y. Ren, M. D. Xiang, L. Z. Li and H. Li, Synthesis of millimeter-scale sponge Fe/Cu bimetallic particles removing TBBPA and insights of degradation mechanism, *Chem. Eng. J.*, 2017, **325**, 279–288, DOI: 10.1016/j.cej.2017.05.018.

51 Z. Huang, D. Y. Deng, J. Q. Qiao, Y. M. Ju, Y. L. Chen and D. D. Dionysiou, New insight into the cosolvent effect on the degradation of tetrabromobisphenol A (TBBPA) over millimeter-scale palladised sponge iron (Pd-s-Fe^0) particles, *Chem. Eng. J.*, 2019, **361**, 1423–1436, DOI: 10.1016/j.cej.2018.10.203.